NASA Technical Memorandum 86699

Kolmogorov and Scalar-Spectral Regimes in Numerical Turbulence

Robert M. Kerr

June 1985

NASA
National Aeronautics and
Space Administration

NASA Technical Memorandum 86699

Kolmogorov and Scalar-Spectral Regimes in Numerical Turbulence

Robert M. Kerr, Ames Research Center, Moffett field, California

June 1985

NASA
National Aeronautics and
Space Administration

Ames Research Center
Moffett Field, California 94035

Kolmogorov and Scalar Spectral Regimes in Numerical Turbulence

ROBERT M. KERR[1]

NASA Ames Research Center
M.S. 202A-1, Moffett Field, CA 94035

ABSTRACT. Velocity and passive-scalar spectra for turbulent fields generated by a forced three-dimensional simulation with 128^3 grid points and Taylor-microscale Reynolds numbers up to 83 are shown to have distinct spectral regimes, including a Kolmogorov inertial subrange. Both one- and three-dimensional spectra are shown for comparison with experiment and theory, respectively. When normalized by the Kolmogorov dissipation scales velocity spectra collapse to a single curve and a high-wavenumber bulge is seen. The bulge leads to an artificially high Kolmogorov constant, but is consistent with recent measurements of the velocity spectrum in the dissipation regime and the velocity-derivative skewness. Scalar spectra, when normalized by the Oboukov-Corrsin scales, collapse to curves which depend only on Prandtl number and show a universal inertial-convective subrange, independent of Prandtl number. When normalized by the Batchelor scales, the scalar spectra show a universal dissipation regime which is independent of Prantl numbers from 0.1 to 1.0. The time development of velocity spectra is illustrated by energy-transfer spectra in which distinct pulses propagate to high wavenumbers.

1. Introduction

The most common tools for describing isotropic, homogeneous turbulence are spectra. In particular, theoretical, experimental, and numerical investigations of the $k^{-5/3}$ inertial subrange of the kinetic-energy spectrum, predicted by Kolmogorov (1941), has become a small industry. The variance spectrum of a passive scalar is also predicted to have an inertial subrange (Oboukov, 1949: Corrsin, 1951). Examples of passive scalars are temperature and salinity, when buoyancy is neglected, and chemical reactants. Experiments strongly support the existence of a $k^{-5/3}$ inertial subrange for both the kinetic-energy and scalar-variance spectra (Champagne (1978) for the velocity and references in Hill (1978) for the scalar).

But the inertial subrange is only one part of the spectra. There are dissipation regimes and for the passive scalar there is an inertial-diffusive regime associated with low Prandtl numbers (high scalar diffusivity) and a diffusive-convective regime associated with high Prandtl numbers (low scalar diffusivity). These regimes are found in wavenumber bands determined by the largest scales of turbulence L (see eq. 16b) and three dissipation scales which depend on the Prandtl number, $Pr = \nu/D$, the viscosity ν, and the kinetic-energy dissipation rate ϵ. The dissipation wavenumbers and corresponding length scales are the Kolmogorov scale,

$$k_k = (\epsilon/\nu^3)^{\frac{1}{4}} = 1/\eta \qquad (1a)$$

[1]Present address: L-387, Lawrence Livermore National Laboratory, P.O. Box 808, Livermore, California 94550

the Batchelor scale,

$$k_B = (\epsilon/\nu D^2)^{\frac{1}{4}} = k_k Pr^{1/2} = 1/\eta_B \tag{1b}$$

and the Oboukov-Corrsin scale,

$$k_{oc} = (\epsilon/D^3)^{\frac{1}{4}} = k_k Pr^{3/4} = 1/\eta_{oc} \tag{1c}$$

The inertial subrange of the kinetic-energy spectrum

$$E(k) = \alpha \epsilon^{2/3} k^{-5/3} \tag{2}$$

where α is the Kolmogorov constant, is found between the turbulent scale L (16b) and the Kolmogorov scale η. Theoretical predictions by Pao (1965) and Herring & Kraichnan (1979) suggest that in the dissipation regime, for $k > k_k$, that the spectrum will decay exponentially with increasing wavenumber.

The inertial-convective subrange of the scalar-variance spectrum

$$E_\theta(k) = \alpha_\theta \chi \epsilon^{-1/3} k^{-5/3} \tag{3}$$

where α_θ is the Oboukov-Corrsin constant, is found between the turbulent scale L and the largest of the dissipation scales, or at wavenumbers below the smallest of the wavenumber cutoffs. For wavenumbers greater than the largest of the wavenumber cutoffs, the scalar spectrum is believed to have an exponential dissipation regime similiar to that for the kinetic-energy spectrum. The spectrum between the inertial-convective subrange and the dissipation regime is determined by the Prandtl number and the ordering of the wavenumber cutoffs.

For high Prandtl number (low diffusivity), the wavenumber cutoffs are ordered as

$$k_k < k_B < k_{oc}$$

and Batchelor (1959) predicts that the viscous-convective spectrum, which is between the Kolmogorov wavenumber and the Batchelor wavenumber, obeys

$$E_\theta(k) = E_\theta(k_k) \frac{k_k}{k} exp(-C_o \frac{D}{e}(k^2 - {k_k}^2)) \sim k^{-1} \tag{4}$$

where e is the root-mean-square rate of strain and $C_o \approx 1$. The exponential with C_o is not rigorous, but Kraichnan (1968) suggests that the k^{-1} power law might be rigorous.

For low Prandtl numbers (high diffusivity) the wavenumber cutoffs are ordered as

$$k_{oc} < k_B < k_k$$

Between k_{oc} and k_k, Batchelor et al. (1959) suggested that the inertial-diffusive spectrum would have the form

$$E_\theta(k) = \frac{\alpha}{3}\chi D^{-3}\epsilon^{2/3}k^{-17/3} \tag{5}$$

Gibson (1968b) predicts that the $k^{-17/3}$ regime will be valid only between k_B and k_k. Between k_{oc} and k_B, that is between the $-17/3$ and $-5/3$ regimes, he predicts another regime which obeys

$$E_\theta(k) = \alpha_G \frac{\chi}{D}k^{-3} \tag{6}$$

Two secondary predictions of Gibson are that the mixed-derivative skewness (27) is independent of Prandtl number (Clay, 1973) and that in the scalar-dissipation regime the spectra for all Prandtl numbers will scale with the Batchelor scales and the strain (Gibson, 1968a). Batchelor (1959) predicted that this scaling would only be true for large Prandtl numbers.

These theoretical results are for three-dimensional spectra. Experimentalists usually present only one-dimensional spectra because single hot-wire anemometers measure only the longitudinal one-dimensional kinetic-energy spectrum

$$E_1'(k_1) = (u_1{}^2(|k_1|) + u_1{}^2(-|k_1|)) \tag{7}$$

With crossed-wire probes the full one-dimensional kinetic-energy spectrum

$$E_1(k_1) = \frac{1}{2}(u^2(|k_1|) + u^2(-|k_1|)) \tag{8}$$

can also measured. In isotropic turbulence these spectra are related to the three-dimensional, kinetic-energy spectrum by

$$E_1'(k_1) = \int_{k_1}^{\infty}(1 - \frac{k_1{}^2}{k^2})\frac{E(k)}{k}dk \tag{9a}$$

$$E(k) = \frac{k^3}{2}\frac{d}{dk}\left(\frac{1}{k}\frac{dE_1'}{dk}\right) \tag{9b}$$

and

$$E_1(k_1) = \int_{k_1}^{\infty}\frac{E(k)}{k}dk \tag{10a}$$

$$E(k) = k\frac{dE_1(k)}{dk} \tag{10b}$$

In the inertial subrange $E_1'(k_1) = \alpha_1'\epsilon^{2/3}k_1^{-5/3}$ and $E_1(k_1) = \alpha_1\epsilon^{2/3}k_1^{-5/3}$, where the one-dimensional Kolmogorov constants are

$$\alpha_1 = \frac{3}{5}\alpha \qquad \alpha_1' = \frac{18}{55}\alpha \tag{11a,b}$$

The one-dimensional scalar-variance spectrum, which can be measured with a single temperature probe, is related to the three-dimensional spectrum by

$$E_{\theta 1}(k_1) = \int_{k_1}^{\infty} \frac{E_\theta(k)}{k} dk \tag{12a}$$

$$E_\theta(k) = k\frac{dE_{\theta 1}(k)}{dk} \tag{12b}$$

In the inertial subrange $E_{\theta 1}(k_1) = \alpha_{\theta 1}\chi\epsilon^{-1/3}k_1^{-5/3}$, where the one-dimensional Oboukov-Corrsin constant is

$$\alpha_{\theta 1} = 0.6\alpha_\theta \tag{13}$$

A major aim of turbulence theory is to successfully predict the constants for these spectral subranges, while an objective of the experimentalists is to provide the theorists with reliable values for the constants. One approach to making theoretical predictions is to use a spectral closure such as the direct-interaction approximation, or DIA, (Kraichnan 1959) or the eddy-damped quasi-normal markovian model (Orszag 1970). Herring and Kraichnan (1979) use a variant of the DIA and calculate the three-dimensional Kolmogorov constant to be 1.85. Larcheveque et al. (1980) review the closure predictions for passive scalars.

Another theoretical approach is to make assumptions about the cascade of energy to high wavenumbers. If the cascade is uniform in space one expects a $k^{-5/3}$ inertial subrange. But it is well known that the cascade is intermittent. Kolmogorov (1962) and Frisch et al. (1978) make assumptions about spatial intermittency and predict small corrections to the $-5/3$ law. Siggia (1978) and Kerr and Siggia (1979) discuss temporal intermittency, but make no spectral predictions.

Measurement and analysis of high-wavenumber velocity spectra is sensitive to errors in instrumentation and in the assumptions of the Taylor "frozen-flow" hypothesis. Only recently have probes been able to measure fluctuations below the Kolmogorov microscale in atmospheric flows and have detailed corrections to the Taylor hypothesis been made. Figure 1 summarizes two sets of experiments. Chapman (1979) cited a variety of older experiments to show a universal Kolmogorov inertial subrange. Detailed corrections to the Taylor hypothesis were not accounted for in these experiments. This should not affect the inertial range strongly, but it will affect the dissipation regime. Champagne (1978) uses the most recent instrumentation and analysis. He finds a Kolmogorov constant which is consistent with Chapman, $\alpha \approx 1.5$ or $\alpha_1' \approx 0.5$, and no significant derivations from the $-5/3$

law are observed. The difference between his dissipation regime and those cited by Chapman is consistent with corrections he made to the Taylor hypothesis. Near the crossover between the inertial and dissipation subranges, Champagne observes a bulge. This is especially large in low-Reynolds-number experiments for the wake behind a cylinder. In addition, the velocity-derivative skewness (see eq. 20) is observed to increase with Reynolds number. Because of a relationship between the spectral shape and the skewness (see eq. 22), a decreasing bulge is consistent with an increasing skewness (see eq. 25).

For the scalar spectrum there is a wide range of scatter in the Oboukov-Corrsin constant, although a value of $\alpha_\theta \approx 1$ or $\alpha_\theta' \approx 0.6$ seems reasonable (Champagne et al. (1977); references in Pao (1965) and Monin and Yaglom (1975), p. 511). For high Prandtl numbers there is strong support for a k^{-1} subrange (see Monin and Yaglom, 1975, p.513), but for low Prandtl numbers there are no reliable measurements because of the exotic nature of the fluids. For $Pr = 0.02$ (liquid mercury), Clay (1973) finds some evidence for a $-17/3$ regime and an intermediate regime which would be consistent with the k^{-3} regime predicted by Gibson (1968b). Experiments in Clay (1973) also support the secondary predictions of Gibson that the mixed-derivative skewness (see eq. 23) will be constant and that the dissipation regime for all Prandtl numbers will obey Batchelor scaling.

Direct numerical simulation of turbulence would seem to be an ideal means of determining the spectra. Conditions can be carefully controlled and because entire fields are available, both one- and three-dimensional spectra can be determined. But until recently these simulations have been restricted by small meshes to very low Reynolds numbers and no inertial regimes have been found. However, Kerr (1985) presents results from a forced spectral simulation with 128^3 mesh points and Taylor-microscale Reynolds number R_λ up to 83. For these flow fields Kerr found a short inertial subrange. We have examined the same flow fields discussed by Kerr (1985) and we will present a larger variety of one- and three-dimensional spectra, including comparisons with theories and experiments.

Figures 1 to 9 depict kinetic-energy and scalar-variance spectra which have been averaged over many flow fields. To study temporal intermittency, time-dependent energy-transfer spectra for some of the same flow fields are presented in figures 10 and 11. Because turbulence is intermittent, one might expect some fluctuations in the time-dependent spectra of a finite sample. In our simulations the turbulent length scale L (see eq. 16b) is the size of the periodic box, so the sample size is very small at the largest turbulent scales, and large fluctuations at low wavenumbers are anticipated. But at the high wavenumbers, or smallest scales, the large mesh size could provide such a large statistical sample that no fluctuations would be observed. The extent of the fluctuations at large wavenumbers indicates the degree to which large-scale intermittency influences the smallest scales of turbulence.

2. Numerical method

The governing equations of the simulation are the incompressible Navier-Stokes equation for the velocity and the transport equation for a passive scalar. The Navier-Stokes equation is

$$\partial u/\partial t + u \cdot \nabla u = -\nabla p/\rho + \nu \nabla^2 u \tag{14}$$

$$\nabla \cdot u = 0 \qquad \text{(incompressibility)}$$

and the convective form of the scalar equation is

$$\partial \vartheta/\partial t + u \cdot \nabla \vartheta = D \nabla^2 \vartheta \tag{15}$$

In the absence of viscosity ν and diffusivity D the equations conserve two positive-definite quadratic invariants: the kinetic energy of turbulent fluctuations,

$$E = \frac{1}{2} < u_i u_i >$$

and the scalar variance,

$$E_\theta = < \theta^2 >$$

The fundamental dimensionless parameters that determine our spectra are the Taylor-microscale Reynolds number, $R_\lambda = U\lambda/\nu$, and the Prandtl number ν/D, where U is the characteristic velocity of the turbulence,

$$\frac{3}{2} U^2 = E$$

and λ is the Taylor microscale,

$$\lambda = < u_1{}^2 >^{1/2} / < (\partial u_1/\partial x_1)^2 >^{1/2}$$

Also of interest are the kinetic-energy dissipation rate,

$$\epsilon = -\frac{d}{dt} < E >$$

the scalar-variance dissipation rate,

$$\chi = -\frac{d}{dt} < E_\theta >$$

and the eddy-turnover time,

$$t_e = \frac{L}{U} \tag{16a}$$

where

$$L = \frac{3\pi}{4E} \int k^{-1} E(k) dk \tag{16b}$$

The numerical code used is a three-dimensional pseudospectral code with periodic boundary conditions. By spectral we mean that the fundamental variables that are stored and advanced in time are the Fourier-transformed velocity and scalar fields, $u(k)$ and $\theta(k)$. Details about the algorithms, aliasing control, and forcing may be found in Kerr (1985). With 128^3 mesh points and no subgrid modeling of the small scales, Taylor-microscale Reynolds numbers as high as 83 can be simulated with full resolution of the smallest scales. Prandtl numbers are restricted in our simulations to less than 1.0 in order to maintain good resolution of the small scales and to greater than 0.1 in order to allow a wide enough range of scales to identify spectral regimes. Details of the simulations are given in the Table 1, with the case numbers corresponding to those in Kerr (1985). For a 128^3 mesh with three scalars approximately 55 seconds of cpu were required per evaluation of the time derivative and 70 hours of Cray-1S time were required for three eddy-turnover times.

To maintain a statistically steady state, the equations were forced by adding energy and scalar variance to the lowest wavenumber band. If the energy cascade is unaffected by the details of the large scales, as assumed by the Kolmogorov hypothesis, then forcing the large scales, or low wavenumbers, should be an effective means of producing small-scale turbulence with many of the same properties as true experimental turbulence. Examination of the spectra is one way in which to test this hypothesis. Figures 1 to 9 represent averages over at least two eddy-turnover times for each Reynolds number.

3. Velocity spectra

Figure 2 presents calculated, three-dimensional, kinetic-energy spectra for several Reynolds numbers. Each point represents the kinetic energy in a spherical shell of wavenumbers between $k = n$ and $n + 1$. The wavenumber plotted is $n + \frac{1}{2}$. One problem with the calculation of the three-dimensional spectrum is that the number of modes in each shell is not a smooth function. To produce a smoother curve, the energy in each shell has been divided by the the number of modes in the shell and multiplied by the volume of the shell, $\frac{4}{3}\pi((n+1)^3 - n^3)$. This has also been done for the scalar-variance spectra in figures 4 to 7. All of the time-averaged spectra to be discussed have been normalized by the Kolmogorov microscales and multiplied by $k^{5/3}$. The inertial subrange would appear as a line with zero slope in these figures.

To be consistent with Kolmogorov hypothesis, all of the simulated spectra should collapse to a single curve. Except for the lowest Reynolds number, all of the spectra in figure 2 do collapse to a single form in the dissipation regime. Below the dissipation regime ($\eta k < 0.4$), the spectra seem to be approaching a limit as the Reynolds number increases. For the largest Taylor-microscale Reynolds number, $R_\lambda = 82.9$, there is a short inertial subrange at the lowest wavenumbers, although not long enough to determine if there are any corrections to Kolmogorov scaling. Since

there are no direct measurements of the three-dimensional kinetic-energy spectrum we can only compare with a theoretical form, such as Pao (see eq. 24), which is shown by the dashed line.

The Kolmogorov constant for the Pao curve is 2.45, which is much higher than the accepted value of 1.5. This value for the Kolmogorov constant could be due to a bulge in the three-dimensional spectrum at the cross-over between the inertial and dissipative regimes. That is, the normalized spectrum appears to drop slightly at the lowest wavenumbers. It is possible that at wavenumbers below those simulated this drop continues, yielding a calculated Kolmogorov constant in better agreement with the experiments. It is also possible that the large Kolmogorov constant is a relic of the low-wavenumber cutoff. In a real flow there is a small backwards transfer of energy associated with vortex pairing. While essentially a two-dimensional process, this also occurs in three dimensions and the low-wavenumber cutoff might block this pairing, forcing excess energy into the high wavenumbers of the simulations. However, if the net energy flow from a true cascade dominates the back transfer, then our forcing can mimic a cascade and the simulation could be calculating the correct Kolmogorov constant for this Reynolds number.

To get better comparisons with experiment, one-dimensional spectra must be plotted. Figure 3 presents the calculated one-dimensional energy spectra (8) for our two highest Reynolds numbers. Pao's form (see eq. 24), integrated by (10a) is shown for two values of the Kolmogorov constant, α=1.7 and α=2.45. At low wavenumbers, the computed spectrum does approach Pao's form for α=1.7, which is near the experimental value of the Kolmogorov constant. Since this spectrum can be measured with crossed-wire probes, some results from Champagne (1978) are included. We took the longitudinal spectrum for a low-Reynolds-number shear flow (his figure 3, R_λ = 130) and added it to twice the cross spectrum for the same flow (his figure 9). While there is no agreement in the inertial subrange, where the effect of the forcing is greatest, the strong agreement in the dissipation range is encouraging. There are small bulges in both the experimental spectrum and the computed spectrum at ηk = 0.2. For better comparisons we encourage experimentalists to measure cross spectra at higher Reynolds number along with the higher-order correlations discussed in Kerr (1985).

Figure 1 presents the calculated, longitudinal, one-dimensional, kinetic-energy spectrum (7) and comparisions with several experiments and curves based on Pao (see eq. 24), integrated by equation (9a). The computed and experimental spectra do not agree in the inertial subrange, but the computed dissipation-range spectrum again agrees with an experiment in Champagne (1978), in this case high-Reynolds-number atmospheric data (his figure 25). Earlier experiments (from Chapman, 1979) strongly dissagree with both the computations and the data from Champagne in the dissipation regime. This discrepancy is consistent with the corrections to the Taylor hypothesis made by Champagne. Neither the computations nor the experiment from Champagne show as large a bulge as the energy spectra in figures

2 and 3, which might explain why this effect had not been noticed in earlier experiments. Lower Reynolds-number experiments for a wake behind a cylinder by Champagne show a larger bulge, but none of the experiments has as large a bulge as our simulations. To understand the relation of this to our results, let us consider the energy-transfer spectrum and the velocity-derivative skewness.

The three-dimensional energy-transfer spectrum

$$T_u(k) \tag{17}$$

is defined by the equation for the three-dimensional kinetic-energy spectrum

$$\frac{d}{dt}E(k) = T_u(k) \; - \nu k^2 E(k) \tag{18}$$

The integral of the energy-transfer spectrum is zero, $\int T_u(k)dk = 0$ (where the limits of all our integrals are from 0 to ∞), but the integral of the vorticity-production spectrum

$$P_\Omega = \int k^2 T_u(k)dk \tag{19}$$

is nonzero and in isotropic turbulence is related to the velocity-derivative skewness

$$S_u = \frac{< \left(\frac{\partial u_1}{\partial x_1}\right)^3 >}{< \left(\frac{\partial u_1}{\partial x_1}\right)^2 >^{\frac{3}{2}}} \tag{20}$$

by

$$-S_{u(k)} = \frac{2}{35}\frac{P_\Omega}{(\frac{\epsilon}{15\nu})^{\frac{3}{2}}} \tag{21}$$

The vorticity production is also related to a fourth-order moment of the kinetic-energy spectrum by an integral equation for the energy dissipation

$$\frac{1}{2\nu}\frac{d}{dt}\epsilon = \int k^2 T_u(k)dk \; - 2\nu \int k^4 E(k)\; dk \tag{22}$$

For our forced simulations, an extra source term should be added, but it appears at low wavenumbers and has negligible effect. Because our simulation is statistically steady, $\frac{d}{dt}\epsilon \rightarrow 0$ and $\int k^2 T_u \rightarrow 2\nu \int k^4 E = \epsilon_\Omega$ as the Reynolds number increases. Therefore, a third measure of the skewness, the dissipation skewness, is (Wyngaard and Tennekes, 1970)

$$-S_\epsilon = \frac{2}{35}\frac{\epsilon_\Omega}{(\frac{\epsilon}{15\nu})^{\frac{3}{2}}} \tag{23}$$

Because of the connection between the skewnesses and the fourth-order moment of the spectra, a simple relation between the velocity-derivative skewness and the Kolmogorov constant exists. If the spectral form of Pao (1965)

$$E(k) = \alpha\epsilon^{2/3}k^{-5/3}exp(-1.5\alpha\nu\epsilon^{-1/3}k^{4/3}) \tag{24}$$

is used with the equation for the velocity-dissipation skewness (23), Kerr (1985) finds

$$S_u = -2.40\alpha^{-3/2} \tag{25}$$

Because Champagne's experiments have shown that Pao's form is a poor representation of the spectrum and because experimental values for the skewness and Kolmogorov constant are not consistent with (25) (Kerr 1985), there is no reason take this equation literally. But it does show that if there is a higher effective Kolmogorov constant, or a larger bulge, the magnitude of the skewness will decrease. Therefore, the decrease in the size of the bulge with Reynolds number is consistent with the observed increase in the skewness in experiments.

Champagne (1978) considered in detail comparisons between S_u and S_ϵ. He found that S_u increases with Reynolds number, possibly approaching -0.8 at very large Reynolds numbers. For our Reynolds number ($\approx$ 83) the values of the simulated skewnesses would be consistent with the experiments, but Kerr (1985) found no evidence that the magnitude of the skewness increases. Both Champagne (1978) and Kerr (1985) found that $S_\epsilon \rightarrow -S_u$ but Kerr (1985) found that the limit of S_ϵ is 0.5, not 0.8. Champagne (1978) also observed that the velocity-derivative flatness

$$F_u = \frac{< \left(\frac{\partial u_1}{\partial x_1}\right)^4 >}{< \left(\frac{\partial u_1}{\partial x_1}\right)^2 >^2} \tag{26}$$

increases with Reynolds number and is related to S_u by

$$\frac{-S_u}{F_u{}^{3/8}} = constant$$

The flatness values in Kerr (1985) are consistent with those of Champagne, but the flatness increases independently of the skewness. The increasing flatness in Kerr (1985) is identified with increasing intermittency at the smallest scales of turbulence. Another inconsistency between the experiment and our simulation is that while the experiments show a larger bulge at low Reynolds number, which is consistent with our simulation, they show no evidence of an inertial subrange, while the simulations do.

These inconsistencies could be due to the forcing. Only in high Reynolds-number experiments, where the small scales might be sufficiently decoupled from the large

scales, could the bulge dissappear and the skewness become constant. In our simulations there is no energy at scales larger than the size of the simulation, so an artificial decoupling might occur and the skewness might reach a maximum earlier and the bulge could remain larger. It is also possible that the skewness does increase with Reynolds number in Kerr (1985), but that the range of Reynolds number is too small to see it. In this case the simulations would be consistent with the experiments.

4. Passive scalar variance spectra

Figures 4 to 6 present three-dimensional scalar-variance spectra for three Prandtl numbers, Pr= 0.1, 0.5, and 1.0, respectively. Four Reynolds numbers are plotted in each case and the spectra are normalized by the variance dissipation, the Kolmogorov microscales, and multiplied by $k^{5/3}$. The spectra have been weighted by the number of modes in the same manner as shown in figure 1. The lowest wavenumber band is not plotted because it is sensitive to the effects of the forcing and does not scale in the manner of the other wavenumbers. Some effects of the forcing are also seen in the lowest plotted wavenumber band in figures 5 and 6, Pr=0.5 and 1.0, for R_λ=82.9. Despite this, as was true for the velocity in figure 1, the scalar-variance spectra in figures 4 to 6 collapse to forms that are independent of Reynolds number in the dissipation regime, except for the lowest Reynolds number. At lower wavenumbers, $\eta k < 0.2$, the spectra seem to be approaching asymptotic forms as the Reynolds number increases.

For low Prandtl number (high diffusivity) there should be an inertial-convective subrange (3) for wavenumbers below the Oboukov-Corrsin cutoff k_{oc}. For simulation F27, Pr=0.1, R_λ = 82.9, and k_{oc} = 8.1. While k_{oc} is within the simulation, it is small and an inertial-convective subrange, which would be indicated by a section with zero slope, is not found in figure 4. The ratio of the Oboukov-Corrsin wavenumber and the Kolmogorov wavenumber for F27 is $\eta k_{oc} = 0.18$, so the regimes predicted by Batchelor et al. (1959) and Gibson (1968b) could also appear. The prediction of Batchelor et al., $k^{-17/3}$ (5), for α=2.45 is shown by the dashed line in figure 4. At low wavenumbers the calculated spectra in figure 4 could be described by an intermediate power law, but not the k^{-3} predicted by Gibson (1968b). Therefore, we must conclude that the Prandtl number of the simulation is not low enough to see any of the predicted low-Prandtl-number spectral regimes. Based on Gibson (1968a,b), Clay (1973) predicted that the mixed-derivative skewness,

$$S_{u\theta} = \frac{< \frac{\partial u_1}{\partial x_1} \left(\frac{\partial \theta}{\partial x_1}\right)^2 >}{< \left(\frac{\partial u_1}{\partial x_1}\right)^2 >^{\frac{1}{2}} < \left(\frac{\partial \theta}{\partial x_1}\right)^2 >} \tag{27}$$

should be independent of Prandtl number. The mixed-derivative skewness is discussed in detail by Kerr (1985), who finds that it is independent of both the Reynolds number and Prandtl number and equal to -0.5 in these simulations, the same value as for the velocity-derivative skewness (20). To get better comparisons with

the theories, lower Prandtl numbers could be simulated, but the Oboukov-Corrsin wavenumber, k_{oc}, would then be in the regime where the forcing dominates and the results would be questionable.

For Pr=0.5 (figure 5) no subranges in the scalar-variance spectrum are expected besides the inertial-convective subrange (3) and the dissipative range. The inertial-convective subrange in figure 5 would be compatible with an Oboukov-Corrsin constant α_θ of about 1.0, or about half the Kolmogorov constant. The one-dimensional constant, $\alpha_{\theta 1} \approx 0.6$ (13), is consistent with the experiments mentioned in the introduction. This is discussed further when direct comparisons to the experiments are made (figure 8).

For large Prandtl number (low scalar diffusivity) Batchelor (1959) predicted a k^{-1} regime such as (4). Pr=1.0 (figure 6) is too low for this subrange to be observed fully, but scalar experiments for Pr=0.7 (air) show a "bump" which looks like a short k^{-1} (Hill, 1978). Therefore, it is not surprising that a significant bump is observed in our calculated spectra for Pr=1.0.

To get a better comparison between the scalar spectra for different Prandtl numbers and the kinetic-energy spectrum, figure 7 presents all the kinetic-energy and scalar spectra for our largest Reynolds number, R_λ=82.9. The effect of the forcing on the first two wavenumber bands is seen for all three Prandtl numbers. That is, if there were no forcing, the the spectra would be smooth at the third wavenumber band.

For comparison with the experiments, one-dimensional scalar-variance spectra for Pr=0.1, 0.5, and 1.0 are presented in figure 8. Only the largest two Reynolds numbers are plotted. An experimental spectrum (Champagne et al. 1977) for Pr=0.7 (air) lies between the calculated spectra for Pr = 0.5 and 1.0, as expected. In the inertial subrange the experimental spectrum is consistent with the calculated spectra for Pr = 0.5 and 1.0, which we expect because scalar dissipation, and the value of the scalar diffusivity D, should not have a significant effect on the inertial-convective subrange.

Gibson (1968a) predicts that in the dissipation regime scalar spectra will depend only upon the scalar dissipation χ, the rate of strain $\frac{\epsilon}{\nu}$, and the Batchelor scale η_B, and be independent of the Prandtl number. With this scaling all of the scalar spectra in the simulations and the experiment of Champagne et. al. (1977) collapse to a single curve in the dissipation regime (figure 9). This agrees with the scaling found in experiments by Clay (1973) for Prandtl numbers from 0.02 (liquid mercury) to 7.0 (water). This prediction is based upon the assumption that at high wavenumbers the large-scale strain can still dominate the scalar dissipation even when the scalar-variance cascade is no longer important. At low Prandtl numbers this can occur only if the rate of strain is constant over scales large compared to Kolmogorov microscale η. This would be consistent with the graphics of Kerr (1985), which show extended vortex structures where the large scale of the vortices is several times η.

5. Energy-transfer spectra

The best means of highlighting temporal fluctuations in the velocity spectrum is to plot the energy-transfer spectrum (17), which indicates the rate at which energy cascades through the spectrum. The time evolution of the transfer spectra for our two largest Reynolds number simulations (F22 and F25) are shown over periods of 1.8 and 1.4 eddy-turnover times in figures 10 and 11, respectively. The time span given in the figures is in simulation variables (see Kerr 1985) and should be compared with the eddy-turnover times in table 1. The transfer in the first wavenumber band (which is always negative) has been divided by its time-averaged value so that it will fit in the figures, and the time-averaged energy-transfer spectrum is given at the top. The time-averaged spectrum is consistent with a Kolmogorov cascade in both figures. In the lowest wavenumber band, which is the energy source, the spectrum is large and negative. At higher wavenumbers the spectrum is positive and almost constant until the dissipation regime. This is expected because the time-averaged transfer spectrum will equal the dissipation spectrum (18) in a statistically steady flow and have a profile similiar to figure 2. As mentioned after (18), the integral of the transfer is zero.

But the time-dependent transfer spectra are not consistent with a steady Kolmogorov cascade. Distinct pulses propagate to higher wavenumbers before disappearing where the dissipation spectrum begins in figure 2 ($k \approx 7$ in figure 10 and $k \approx 10$ in figure 11). Their progress is outlined by dotted lines in figure 11. The pulses are characterized by a positive leading, or high wavenumber, part and a negative following part, superimposed on the constant positive background. The rate at which they propagate to high wavenumber appears to be linear with time, but the sample is small. There is no indication that they would propagate to infinite wavenumber in a finite time if the viscosity were zero.

Despite the large statistical sample at moderate wavenumbers ($k \leq 10$) in the 128^3 simulation (figure 11), the pulses remain distinct until the dissipation regime. If statistics alone governed the size of the pulses, one might expect that their strength would decay as the square root of the sample size. Since the size of each wavenumber shell goes as k^2, this would imply that the pulses should decay as k^{-1}. It is clear that they do not. Therefore large-scale intermittency is felt in the dissipation regime. This would be consistent with the vortex structures observed in Kerr (1985) that extend from the largest scales of these simulations to the Kolmogorov microscale. Note that a $k^{-5/3}$ spectrum occurs in our simulation along with large temporal and spatial intermittency. This suggests that intermittency can be consistent with a $k^{-5/3}$ inertial regime and does not necessarily lead to corrections of the type predicted by Kolmogorov (1962) and Frisch et al. (1978). Lundgren (1982) has a model for dissipation structures that is based upon strained vortex tubes similiar to those observed by Kerr (1985). His model develops a $k^{-5/3}$ spectrum when fluctuation pulses are averaged in time.

Similiar pulses have been observed before for time-dependent spectra in simple

spectral models. Kerr and Siggia (1978) present a cascade model of turbulence where each band of wavenumbers with $2^{l-1} < |k| \leq 2^l$ is modeled by a single complex variable. They observed pulses of energy cascading to high wavenumbers, then dissipating. But there are some significant differences between their model and the Navier-Stokes equation, in addition to the severe wavenumber truncation. They found an extra third-order quantity, in addition to the energy, which was nonzero and conserved by the nonlinear terms. The only analog to this term in the Navier-Stokes equation is the energy-transfer spectrum, whose integral is zero. They also showed that their model could be derived from a truncated form of Burgers equation. Burgers equation is a one-dimensional equation that is known to form shocks, which do not exist in an incompressible flow. The pulses in Kerr and Siggia were identified with these shocks. Nonetheless, the envelopes of the pulses in Kerr and Siggia, when plotted in terms of the third-order invariant, and of the pulses in the energy-transfer spectra seen in figures 10 and 11 are similiar and suggest that the pulses might be identified with the development of sharp structures in the velocity or vorticity field. The appearance of extended vortex structures in the graphics of Kerr (1985) might represent this process.

Our simulation and the latest experiments observe a high-wavenumber bulge, while steady spectral closures do not. Because the net transfer spectrum is given by the dissipation spectrum through (18), the bulge implies that energy transfer into a wavenumber regime through the nonlinear terms decreases more slowly with increasing wavenumber than transfer out of that regime. This could mean that temporal or spatial intermittency could provide a mechanism which would explain this and the bulge. A steady, not just statistically steady, cascade would not suffice because the rates of energy transfer into and out of a wavenumber regime should decay together with increasing wavenumber. However, a strong pulse could transfer energy into the dissipation regime faster than it is removed by dissipation. The rate at which a pulse transfers energy into the dissipation regime goes as η/U, where U is the strength of the pulse and η is the Kolmogorov or dissipation microscale (1a). If viscous diffusion prevents the nonlinear terms from transferring energy to higher wavenumbers, then the pulse can decay only through viscous dissipation, with timescale τ_K. For a sufficiently strong pulse, U could be large enough that the transfer into the dissipation scales would be faster than the viscous dissipation and a bulge would be produced. This might be similiar to the turnup at the high wavenumber end of time-averaged spectra (figures 1-9), which occurs because there are no wavenumbers beyond the high-wavenumber spectral cutoff for energy to drain into.

6. Conclusion

We have studied in detail spectra produced by numerical simulation of the incompressible Navier-Stokes equations and passive-scalar transport equations for a range of Reynolds numbers and Prandtl numbers. These simulations are limited by the mesh size to moderate Reynolds numbers, and an artificial forcing was used

to maintain a statistically steady state. With these qualifications, we believe that this is the first time a Kolmogorov inertial subrange has been directly simulated for an extensive period. In other cases where a Kolmogorov spectrum has been found either subgrid modeling was used (Siggia and Patterson, 1978) or the spectrum was transient (Brachet et al. 1983). The Kolmogorov constant that we found is too large, but from comparisons with experimental values at low Reynolds number it seems probable that when higher Reynolds numbers can be simulated, better agreement will be obtained. In particular, the high-wavenumber bulge might decrease with increasing Reynolds number while the velocity-derivative skewness increases, as observed in some experiments. The close agreement between the simulations and the experiments of Champagne (1978) in the dissipation regime is encouraging.

Scalar-variance spectra are believed to have two spectral regimes which depend on Prandtl number, in addition to regimes similiar to the inertial subrange and the dissipation regime found for the velocity. The simulations are consistent with these predictions, but the range of Prandtl numbers is too small to allow direct comparisons with either the very high or very low Prandtl number theories. While there is no solid evidence as to whether the Batchelor et al. (1959) or the Gibson (1968b) theory for the spectral form at small Prandtl numbers is correct, two secondary predictions based on Gibson (1968a,b) are supported; the mixed-derivative skewness is constant and the scalar-dissipation spectra obey Batchelor scaling.

Pulses are observed in the energy-transfer spectrum which have a profile similiar to those observed in the cascade model of Kerr and Siggia (1978). The pulses propagate linearly in time to high wavenumbers and are distinct until the dissipation regime. This would suggest that large-scale intermittency is felt at the smallest scales and is consistent with the vortex structures found in the graphics of Kerr (1985). The appearance of a Kolmogorov inertial subrange, along with extended small-scale structures and spectral pulses is consistent with the model of Lundgren (1982). The pulses and the extended structures could provide a mechanism for allowing energy to cascade further into the dissipation regime than is predicted by spectral closures, which would explain the bulge in the kinetic-energy spectrum.

The simulations which produced the spectra were the largest possible on present computers. Despite the limitations, satisfactory comparisons with experiments were obtained and some new insight was gained. As computer speed and memory increases, we are certain that these results will be extended to higher Reynolds numbers and a wider range of Prandtl numbers, and that eventually it will be unnecessary to use an artificial forcing to reach these Reynolds numbers.

I wish to thank C.H. Gibson and R. S. Rogallo for many useful discussions.

REFERENCES

Batchelor, G. K. 1959 Small-scale variation of convected quantities like temperature in turbulent fluid. Part 1. General discussion and the case of small conductivity. J. Fluid Mech. 5, 113-133.

Batchelor, G. K., Howells, I. D. & Townsend, A. A. 1959 Small-scale variation of convected quantities like temperature in turbulent fluid. Part 2. The case of large conductivity. J. Fluid Mech. 5, 134-139.

Brachet, M.E., Meiron, D.I., Orszag, S.A., Nickel, B.G., Morf, R.H. & Frisch, U. 1983 Small-scale structure of the Taylor-Green vortex. J. Fluid Mech. 130, 411-452.

Champagne, F.H. 1978 The fine-scale structure of the turbulent velocity field. J. Fluid Mech. 86, 67-108.

Champagne, F. H., Friehe, C. A., LaRue, J. C., & Wyngaard, J. C. 1977 Flux measurements, flux estimation techniques and fine-scale turbulence measurements in the unstable surface layer over land. J. Atmos. Sci. 34, 515.

Chapman, D.R. 1979 Computational aerodynamics development and outlook. A.I.A.A.J. 17, 1293-1313.

Clay, J. P. 1973 Turbulent mixing of temperature in water, air and mercury. Ph.D. thesis, University of California at San Diego.

Corrsin, S. 1951 On the spectrum of isotropic temperature fluctuations in isotropic turbulence. J. Appl. Phys. 22, 469-473.

Frisch, U., Sulem, P. L. & Nelkin, M. 1979 A simple model of intermittent fully developed turbulence. J. Fluid Mech. 87, 719-736.

Gibson, C. H. 1968a Fine structure of scalar fields mixed by turbulence. I. Zero-gradient points and minimal-gradient surfaces. Phys. Fluids 11, 2316-2327.

Gibson, C. H. 1968b Fine structure of scalar fields mixed by turbulence. II. Spectral theory. Phys. Fluids 11, 2316-2327.

Herring, J.R. & Kraichnan, R.H. 1979 A numerical comparison of velocity-based and strain-based Lagrangian-history turbulence approximations. J. Fluid Mech. 89, 581-597.

Hill, R. J. 1978 Models of the scalar spectrum for turbulent advection. J. Fluid Mech. 88, 541-562.

Kerr, R. M. 1985 Higher-order derivative correlations and the alignment of small-scale structures in isotropic numerical turbulence. J. Fluid Mech. 153, 31-58. (see also NASA TM 84407, 1983.)

Kerr, R.M. & Siggia, E.D. 1978 Cascade mode of fully developed turbulence. J. Stat Phys. 19, 543-552.

Kolmogorov, A. N. 1941 Local structure of turbulence in an incompressible fluid at very high Reynolds numbers. C. R. Acad. Sci. UUSR 30, 301-305.

Kolmogorov, A. N. 1962 A refinement of previous hypotheses concerning the local structure of turbulence in a viscous incompressible fluid at high Reynolds number. J. Fluid Mech. 13, 82-85.

Kraichnan, R.H. 1959 The structure of isotropic turbulence at very high Reynolds numbers. J. Fluid Mech. 5, 497-543.

Kraichnan, R.H. 1968 Small-scale structure of a scalar field convected by turbulence. Phys. Fluids 11, 945-953.

Larcheveque, M., Chollet, J. P., Herring, J. R., Lesieur, M., Newman, G. R.

& Schertzer, D. 1980 Two-point closure applied of a passive scalar in decaying isotropic turbulence. In Turbulent Shear Flows 2 (eds. J. S. Bradbury, F. Durst, B. E. Launder, F. W. Schmidt & J. H. Whitelaw), pp. 50-60. Springer.

Lundgren, T. S. 1982 Strained spiral vortex model for turbulent fine structure. Phys. Fluids 25, 2193-2203.

Monin, A.S. & Yaglom, A.M. 1975 Statistical Fluid Mechanics, vol. 2. Massachusetts Institute of Technology Press.

Oboukov, A.M. 1949 Structure of the temperature field in a turbulent flow. Izv. Akad. Nauk. SSSR, Ser. Geogr. i Geofiz. 13, 58-69.

Orszag, S.A. 1970 Analytical theories of turbulence. J. Fluid Mech. 41, 363-386.

Pao, Y-H. 1965 Structure of turbulent velocity and scalar fields at large wavenumbers. Phys. Fluids 8, 1063-1075.

Siggia, E.D. 1978 Model of intermittency in three-dimensional turbulence. Phys. Rev. A17, 1166-1176.

Siggia, E. D. & Patterson, G. S. 1978 Intermittency effects in a numerical simulation of stationary three-dimensional turbulence. J. Fluid Mech. 86, 567-592.

Wyngaard, J.C. & Tennekes, H. 1970 Measurements of the small-scale structure of turbulence at moderate Reynolds numbers. Phys. Fluids 13, 1962-1969.

Table 1

Characteristics of the Simulations

Run	Mesh	R_λ	Pr	k_k	k_B	k_{oc}	t_e
F6	32^3	18.5	1.0	16.5	16.5	16.5	1.97
F7	32^3	"	0.5	"	11.7	9.8	"
F8	32^3	"	0.1	"	5.2	2.9	"
F16	64^3	37.5	1.0	16.0	16.0	16.0	2.51
F17	64^3	"	0.5	"	11.3	9.5	"
F18	64^3	"	0.1	"	5.1	2.8	"
F19	64^3	48.2	1.0	22.4	22.4	22.4	1.41
F20	64^3	"	0.5	"	15.8	13.3	"
F21	64^3	"	0.1	"	7.1	4.0	"
F22	64^3	55.9	1.0	27.2	27.2	27.2	1.05
F23	64^3	"	0.5	"	19.2	16.2	"
F24	64^3	"	0.1	"	8.6	4.8	"
F25	128^3	82.9	1.0	45.7	45.7	45.7	0.85
F26	128^3	"	0.5	"	32.3	27.2	"
F27	128^3	"	0.1	"	14.5	8.1	"

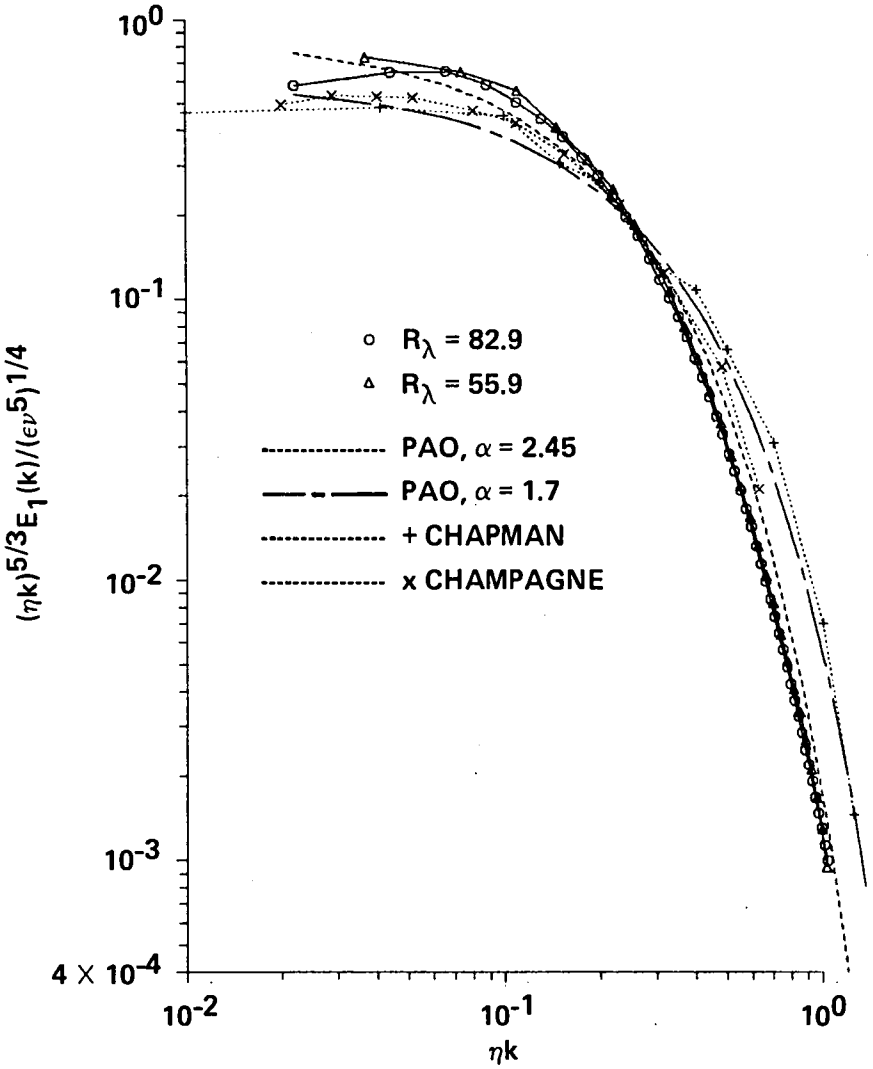

Figure 1: Longitudinal one-dimensional kinetic-energy spectra (5) normalized by the Kolmogorov microscales and multipied by $k^{5/3}$. Circle: $R_\lambda = 82.9$. Triangle: $R_\lambda = 55.9$. Curves based on Pao's theoretical form (1). integrated by (8a) for $\alpha = 2.45$ and $\alpha = 1.7$ are indicated by the dashed and long-dashed lines respectively. The one-dimensional Kolmogorov constant is $\alpha_1' = \frac{18}{55}\alpha$. Experimental spectra from Chapman (1979) (plus) and Champagne (1978) (cross) are indicated with dotted lines.

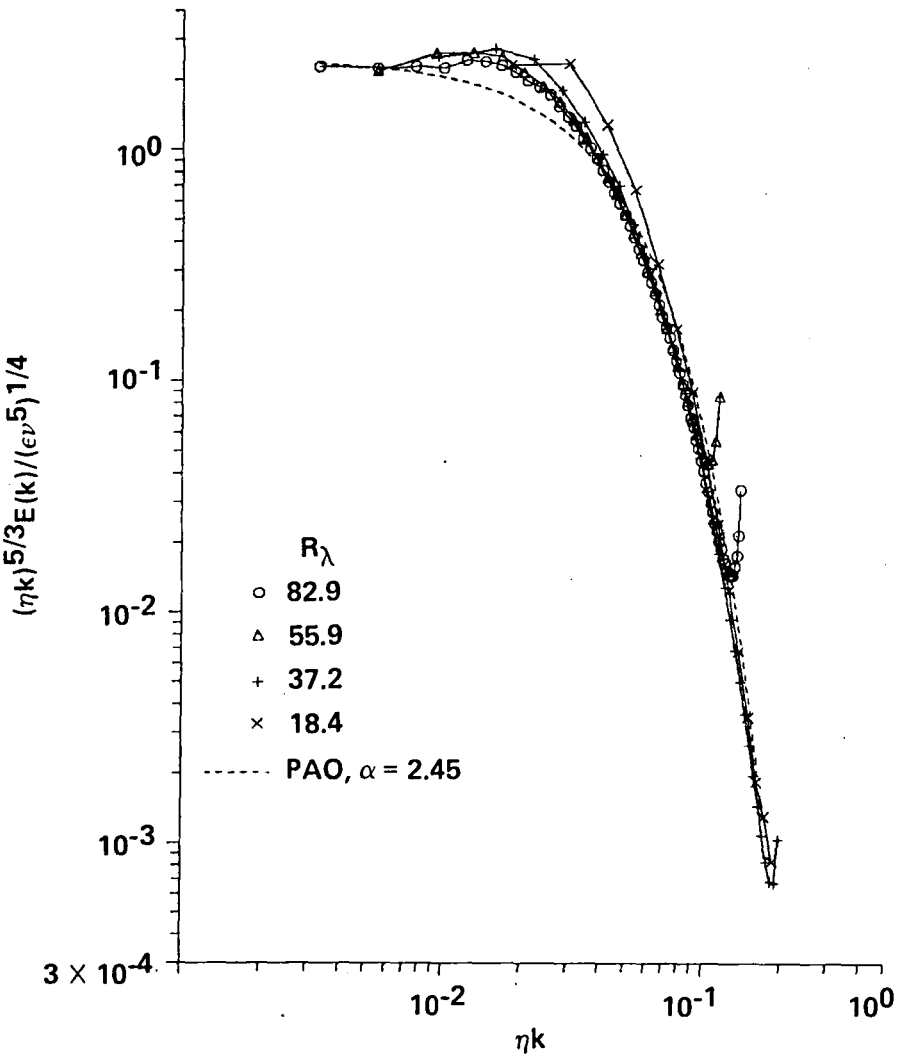

Figure 2: Three-dimensional kinetic-energy spectra normalized by the Kolmogorov microscales and multipied by $k^{5/3}$. Circle: $R_\lambda = 82.9$. Triangle: $R_\lambda = 55.9$. Plus: $R_\lambda = 37.2$. Cross: $R_\lambda = 18.4$. Pao's theoretical form (1) for $\alpha = 2.45$ is indicated by the dashed line.

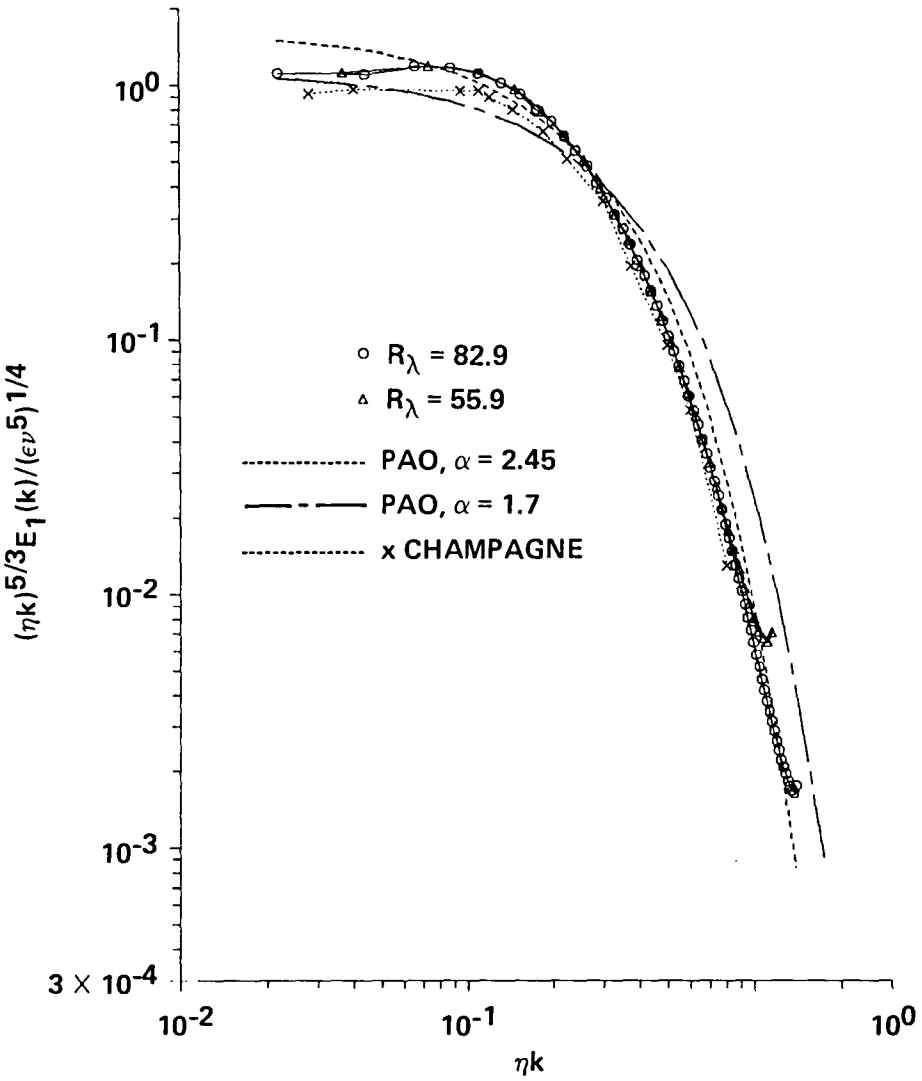

Figure 3: One-dimensional kinetic-energy spectra (6) normalized by the Kolmogorov microscales and multipied by $k^{5/3}$. Circle: $R_\lambda = 82.9$. Triangle: $R_\lambda = 55.9$. Curves based on Pao's theoretical form (1), integrated by (8a) for $\alpha = 2.45$ and $\alpha = 1.7$ are indicated by the dashed and long-dashed lines respectively. The one-dimensional Kolmogorov constant is $\alpha_1 = 0.6\alpha$. An experimental spectrum from Champagne (1978) is indicated by the dotted line.

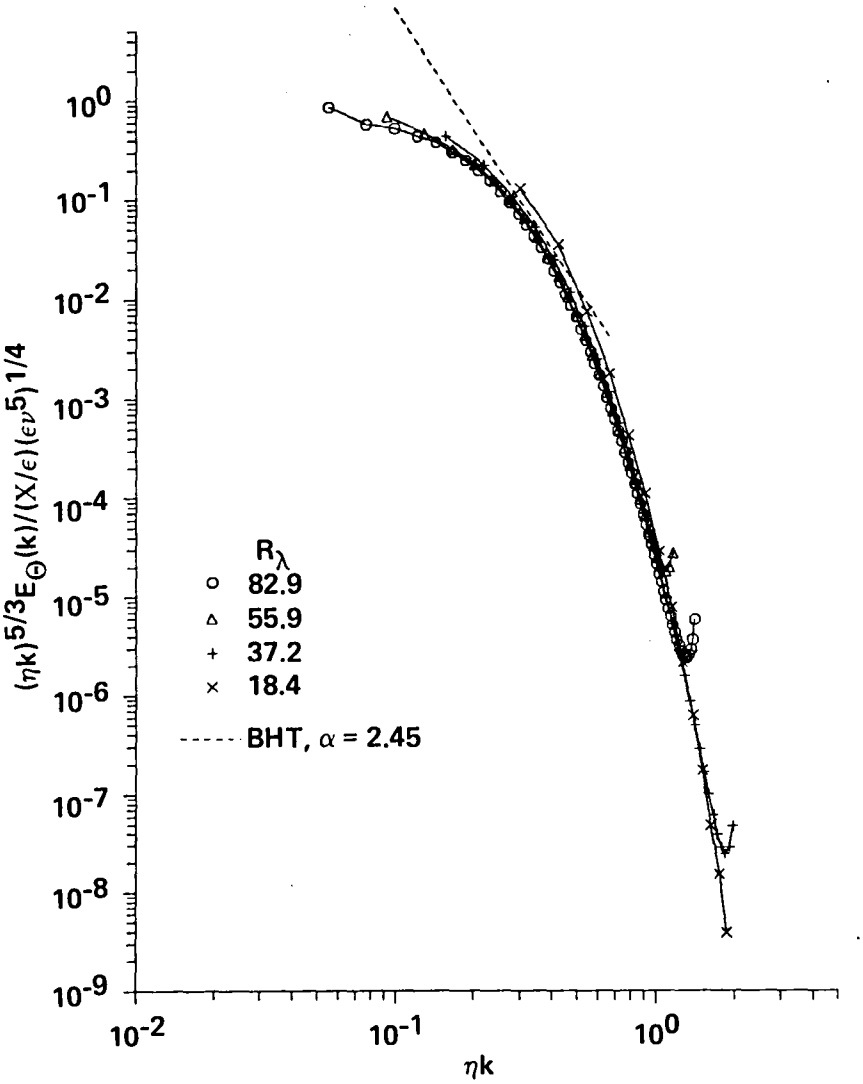

Figure 4: Three-dimensional scalar-variance spectra for $Pr = 0.1$ normalized by the Kolmogorov microscales and the scalar-variance dissipation χ and multipied by $k^{5/3}$. The lowest mode is not plotted. Circle: $R_\lambda = 82.9$. Triangle: $R_\lambda = 55.9$. Plus: $R_\lambda = 37.2$. Cross: $R_\lambda = 18.4$. The prediction of Batchelor et al. (1959) (4), k^{-173} for $\alpha = 2.45$, is shown by the dashed line.

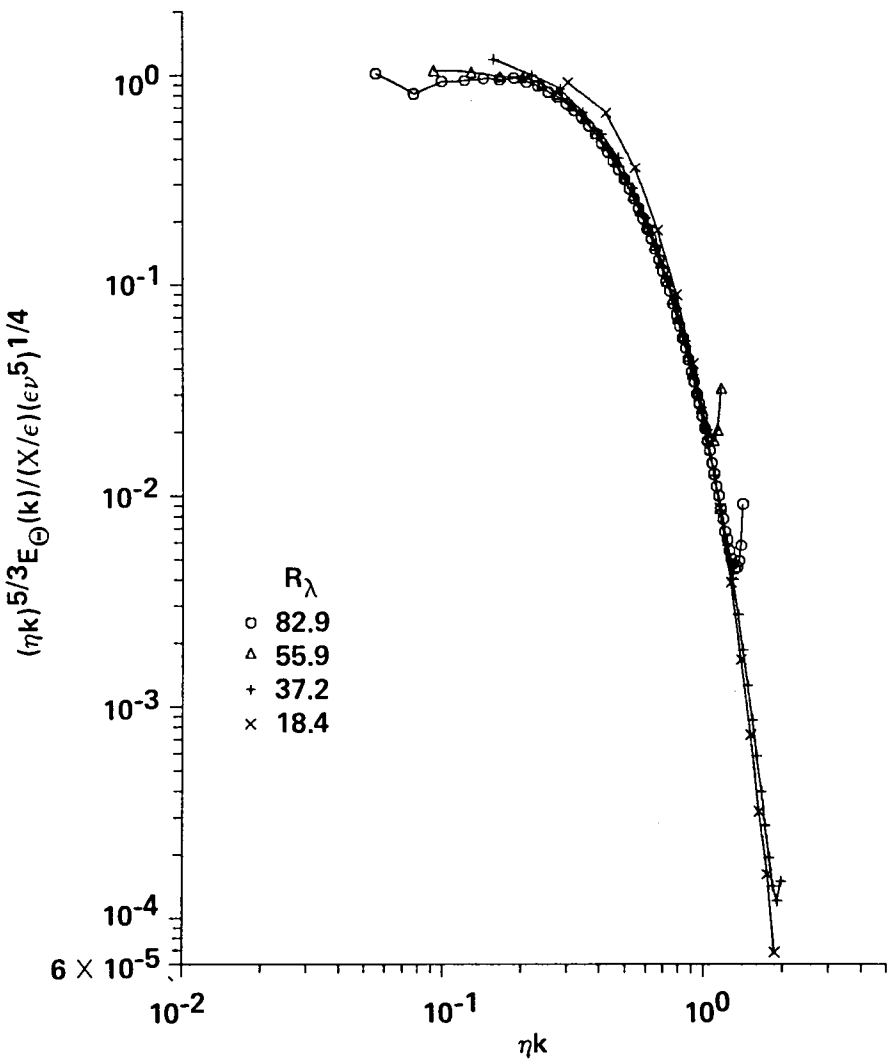

Figure 5: Three-dimensional scalar-variance spectra for $Pr = 0.5$ normalized by the Kolmogorov microscales and the scalar-variance dissipation χ and multipied by $k^{5/3}$. The lowest mode is not plotted. For symbols see figure 4.

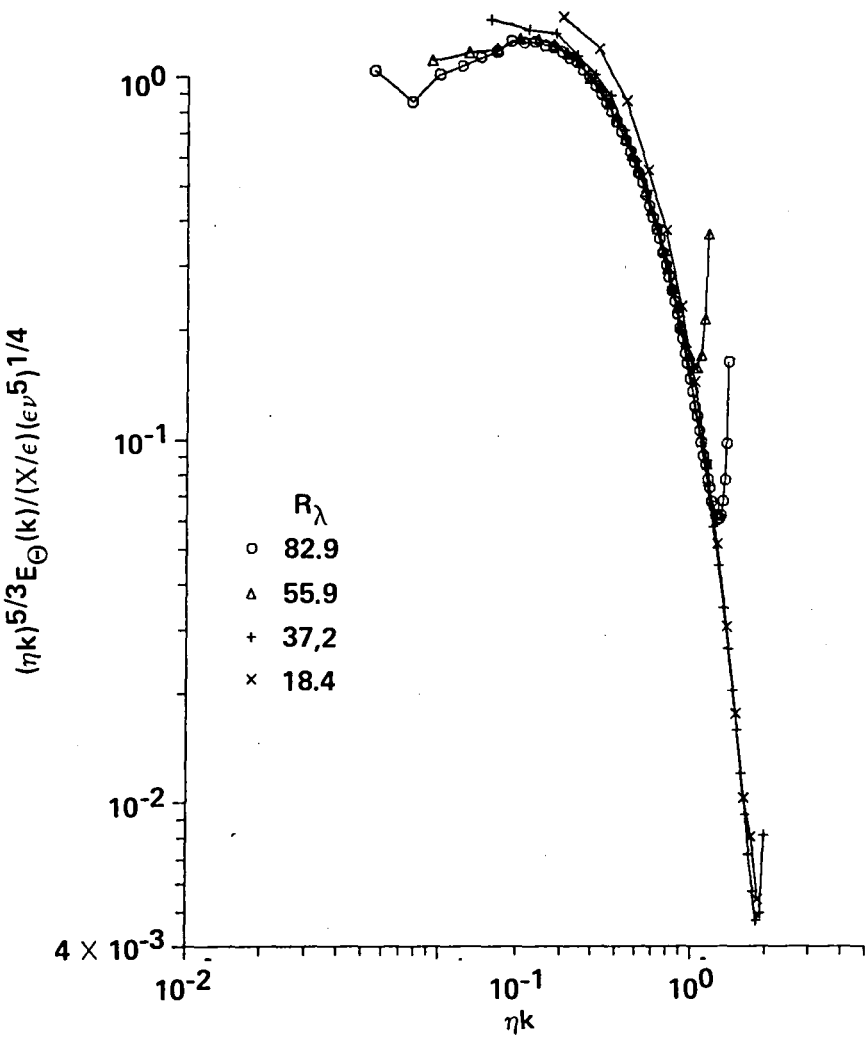

Figure 6: Three-dimensional scalar-variance spectra for $Pr = 1.0$ normalized by the Kolmogorov microscales and the scalar dissipation χ and multipied by $k^{5/3}$. The lowest mode is not plotted. For symbols see figure 4.

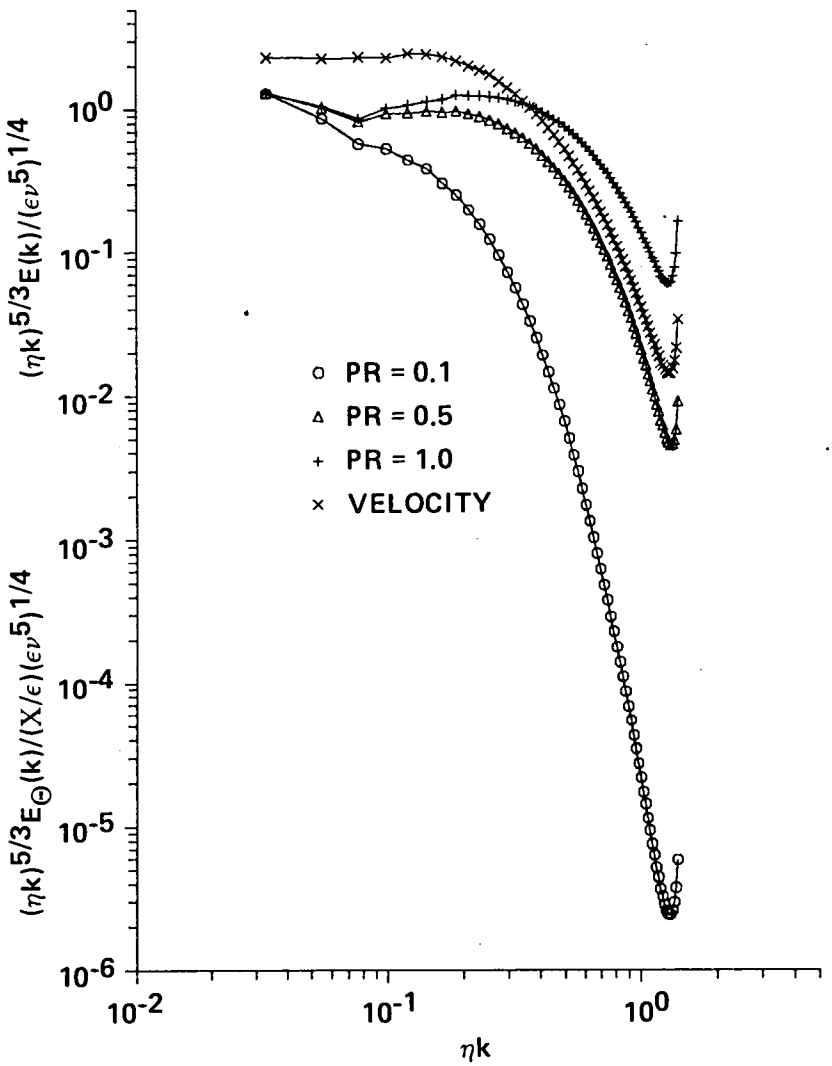

Figure 7: Three-dimensional kinetic-energy and passive-scalar spectra for R_λ=82.9, normalized by the Kolmogorov microscales and the scalar-variance dissipation χ, and multipied by $k^{5/3}$. The lowest mode is plotted. Circle: Pr=0.1. Triangle: Pr=0.5. Plus: Pr=1.0. Cross: Kinetic energy.

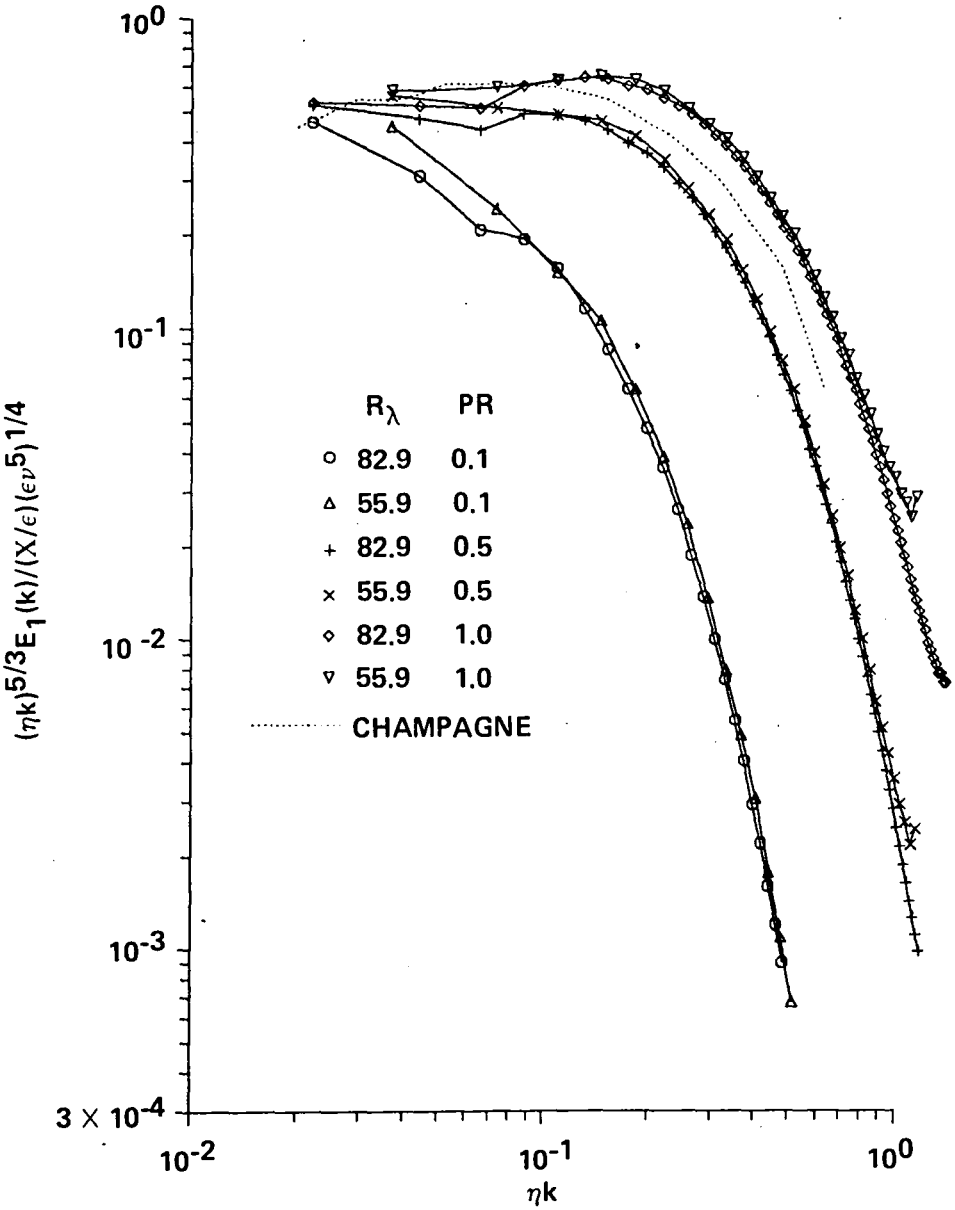

Figure 8: One-dimensional scalar-variance spectra normalized by the Kolmogorov microscales and the scalar-variance dissipation χ and multipied by $k^{5/3}$. Circle: R_λ = 82.9 and Pr = 0.1. Triangle: R_λ = 55.9 and Pr = 0.1. Plus: R_λ = 82.9 and Pr = 0.5. Cross: R_λ = 55.9 and Pr = 0.5. Diamond: R_λ = 82.9 and Pr = 1.0. Inverted triangle: R_λ = 55.9 and Pr = 1.0. Experimental spectrum from Champagne et al. (1977) (dotted line).

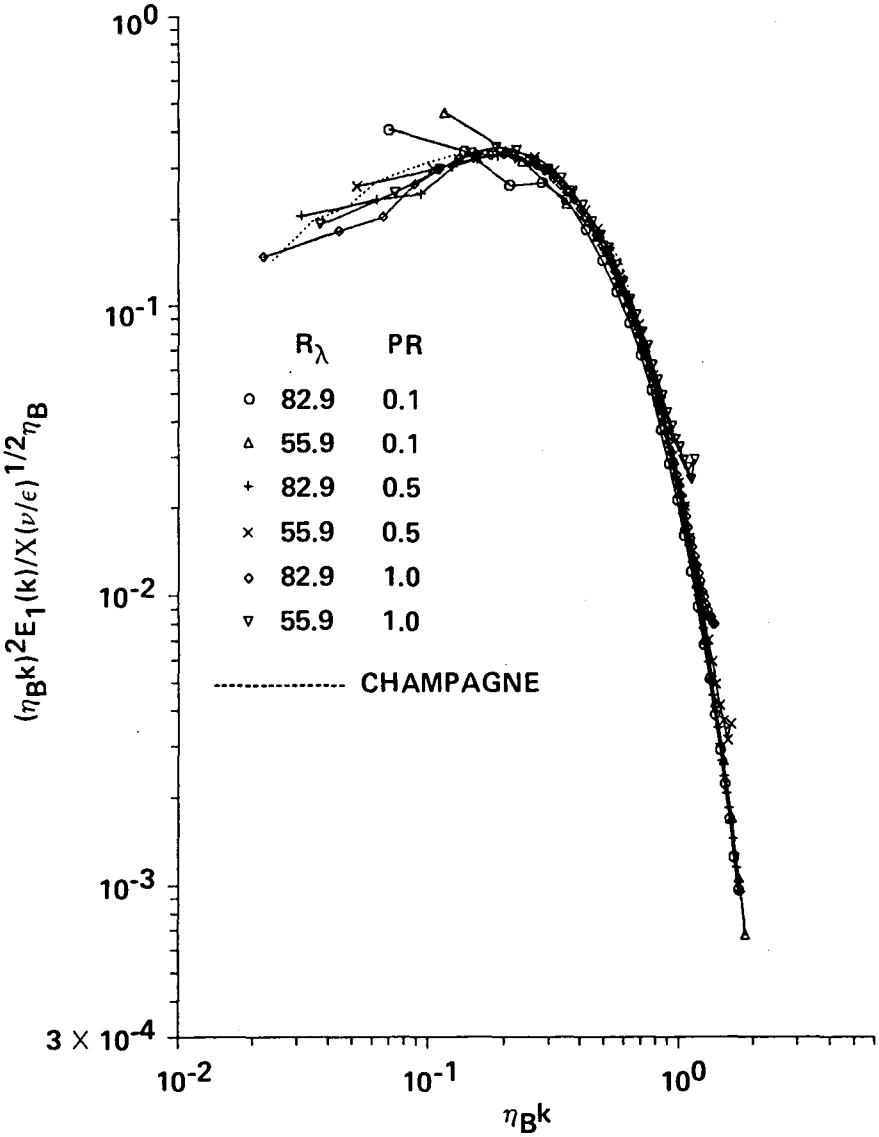

Figure 9: One-dimensional scalar-dissipation spectra normalized by the Batchelor microscale, the scalar-variance dissipation χ and the rate of strain $\frac{\epsilon}{\nu}$. For symbols see figure 8.

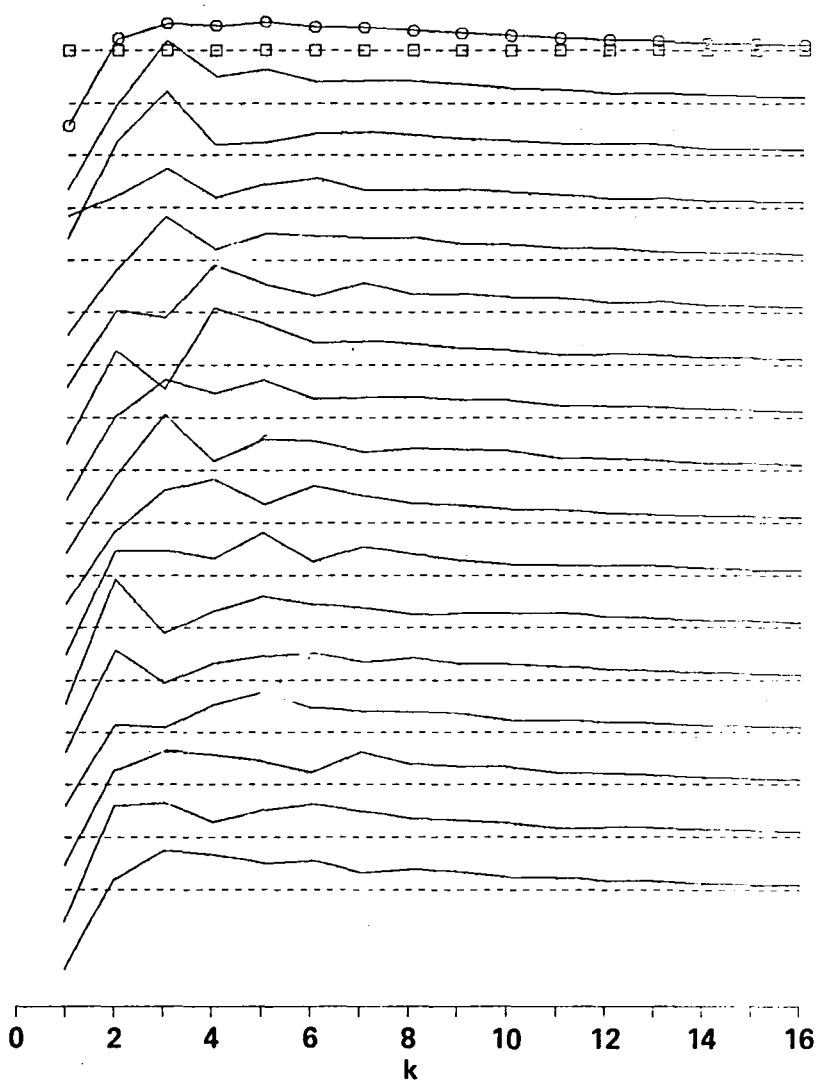

Figure 10: Three-dimensional kinetic-energy transfer spectra for discrete times for simulations F22-24, $R_\lambda = 55.9$. Dashed lines indicate the wavenumber axis for each time. Solid lines indicate the spectra. Squares are the wavenumber axis for the time-averaged transfer spectrum. Circles are the time-averaged spectrum. The lowest mode for each spectrum is normalized by its time-averaged value. The figure spans simulation times from t=1.125 to 3.0, with time increasing from bottom to top. This should be compared with the eddy turnover time in Table 1.

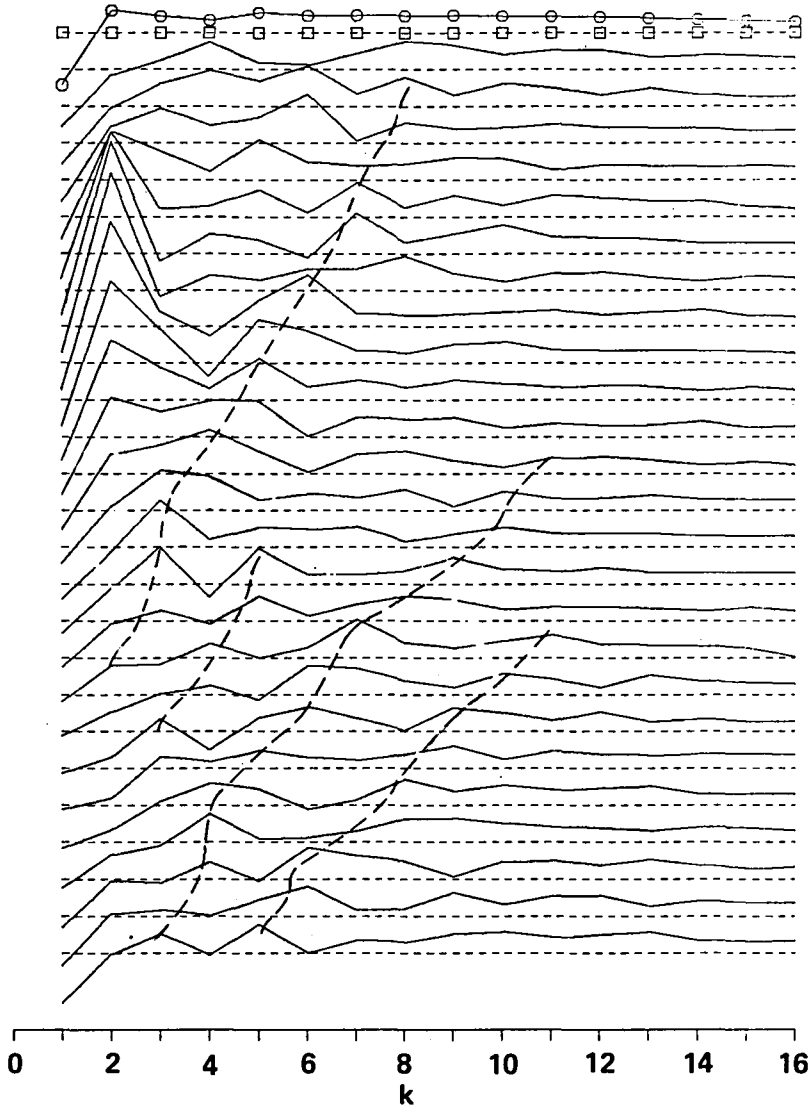

Figure 11: Three-dimensional kinetic-energy transfer spectra for discrete times for simulations F25-27, $R_\lambda = 82.9$. Dashed lines indicate the wavenumber axis for each time. Solid lines indicate the spectra. Squares are the wavenumber axis for the time-averaged transfer spectrum. Circles are the time-averaged spectrum. The lowest mode for each spectrum is normalized by its time-averaged value. The figure spans simulation times from t=2.10 to 3.3, with time increasing from bottom to top. This should be compared with the eddy turnover time in Table 1. (Dotted lines indicate where pulses are moving to higher wavenumber.)

1. Report No.	2. Government Accession No.	3. Recipient's Catalog No.
NASA TM-86699		

4. Title and Subtitle	5. Report Date
KOLMOGOROV AND SCALAR SPECTRAL REGIMES IN NUMERICAL TURBULENCE	June 1985
	6. Performing Organization Code

7. Author(s)	8. Performing Organization Report No.
Robert M. Kerr	85160
	10. Work Unit No.

9. Performing Organization Name and Address	11. Contract or Grant No.
Ames Research Center Moffett Field, CA 94035	
	13. Type of Report and Period Covered
12. Sponsoring Agency Name and Address	Technical Memorandum
National Aeronautics and Space Administration Washington, DC 20546	14. Sponsoring Agency Code 505-31-01-01-00-21

15. Supplementary Notes

Point of contact: Harvard Lomax, Ames Research Center, MS 202A-1, Moffett Field, CA 95035, (415)694-5124 or FTS 464-5124

16. Abstract

Velocity and passive-scalar spectra for turbulent fields generated by a forced three-dimensional simulation with 128^3 grid points and Taylor-microscale Reynolds numbers up to 83 are shown to have distinct spectral regimes, including a Kolmogorov inertial subrange. Both one- and three-dimensional spectra are shown for comparison with experiment and theory, respectively. When normalized by the Kolmogorov dissipation scales velocity spectra collapse to a single curve and a high-wavenumber bulge is seen. The bulge leads to an artificially high Kolmogorov constant, but is consistent with recent measurements of the velocity spectrum in the dissipation regime and the velocity-derivative skewness. Scalar spectra, when normalized by the Oboukov-Corrsin scales, collapse to curves which depend only on Prandtl number and show a universal inertial-convective subrange, independent of Prandtl number. When normalized by the Batchelor scales, the scalar spectra show a universal dissipation regime which is independent of Prandtl numbers from 0.1 to 1.0. The time development of velocity spectra is illustrated by energy-transfer spectra in which distinct pulses propagate to high wavenumbers.

17. Key Words (Suggested by Author(s))	18. Distribution Statement
Turbulence Numerical Simulation Mixing Chaos Statistical Physics	Unlimited Subject Category - 34

19. Security Classif. (of this report)	20. Security Classif. (of this page)	21. No. of Pages	22. Price*
Unclassified	Unclassified	31	A03

*For sale by the National Technical Information Service, Springfield, Virginia 22161

End of Document